

Contents lists available at ScienceDirect

Palaeogeography, Palaeoclimatology, Palaeoecology

journal homepage: www.elsevier.com/locate/palaeo



Sulfate-driven anaerobic oxidation of methane recorded by Lower Cretaceous (Barremian) authigenic carbonate deposits from the Kuhnpasset Beds of Wollaston Forland, northeast Greenland

Siyu Wang ^{a,b}, Daniel Birgel ^{b,*}, Hans Arne Nakrem ^c, Crispin T.S. Little ^d, Øyvind Hammer ^c, Simon R.A. Kelly ^{e,1}, Jörn Peckmann ^{b,*}

- a Key Laboratory of Tectonics and Petroleum Resources, Ministry of Education, China University of Geosciences, Wuhan 430074, China
- ^b Department of Earth System Sciences, University of Hamburg, 20146 Hamburg, Germany
- ^c Natural History Museum, University of Oslo, PO Box 1172, Blindern, NO-0318 Oslo, Norway
- ^d School of Earth and Environment, University of Leeds, Leeds LS2 9JT, United Kingdom
- ^e CASP, West Building, Madingley Rise, Madingley Road, Cambridge CB3 0UD, United Kingdom

ARTICLE INFO

Editor name: Dr. Howard Falcon-Lang

Keywords:
Seep carbonates
Anaerobic oxidation of methane
Lipid biomarkers
Wood fragments
Lower Cretaceous
Northeast Greenland

ABSTRACT

The Lower Cretaceous (Barremian) Kuhnpasset sedimentary sequence of northeast Greenland contains many carbonate deposits in different stratigraphic positions in the area of Wollaston Forland, several of which have previously been identified as having a hydrocarbon seep origin based on their macrofossil content and morphology. Most of the seep carbonates contain complex internal microfabrics, including abundant yellow calcite and banded and botryoidal cement with δ^{13} C values as low as -54 ‰. These δ^{13} C values are characteristic of carbonate microfabrics with biogenic methane as the major carbon source and carbonate authigenesis caused by sulfate-driven anaerobic oxidation of methane (SD-AOM). Such ¹³C-depletion confirms a methane seep origin of most of the Kuhnpasset carbonate deposits. Molecular fossils from the seep carbonates prove methanotrophic archaea were involved in the SD-AOM consortia, based on ¹³C-depleted 2,6,10,15,19-pentamethylicosane (PMI; δ^{13} C: -122 to -113 %) and the co-eluting crocetane and phytane (-124 to -105 %). The carbon source for the Kuhnpasset seeps was biogenic methane with a δ^{13} C value of approximately -70 ‰, as calculated from compound-specific δ^{13} C values of archaeal lipid biomarkers. The δ^{13} C values of the biomarkers of sulfatereducing bacteria, the synthrophic partners of archaea in SD-AOM, including iso- and anteiso-C15/17 fatty acids are less 13 C-depleted (-107 to -87 %) than the archaeal biomarkers - a pattern known from modern seep environments. Preservation of bacterial fatty acids is rare for Mesozoic seep deposits, revealing excellent biomarker preservation and low thermal maturity of the Kuhnpasset seep deposits. The common isoprenoid hydrocarbon biomarkers of SD-AOM in the Kuhnpasset seep carbonates are accompanied by ¹³C-depleted isoprenoic acids (phytanoic acid: -112 to -101 %); these compounds are attributed to the early degradation of glycerol diether membrane lipids such as archaeol or sn2-hydroxyarchaeol, which are not preserved in the samples. Similarly, regular PMI-acid (-120 to -107 %) probably represents a derivative of extended archaeol or extended hydroxyarchaeol. The molecular fossil inventories in the Kuhnpasset seep carbonates and the predominance of early diagenetic banded and botryoidal cement are characteristic of the dominance of ANME-2 consortia adapted to high methane flux with the sulfate-methane transition zone (SMTZ) positioned at shallow sediment depth. Abundant wood fragments and well-preserved leafy conifer shoots enclosed in the Kuhnpasset seep deposits indicate a shallow marine paleoenvironment of deposition close to the former shoreline.

^{*} Corresponding authors.

E-mail addresses: daniel.birgel@uni-hamburg.de (D. Birgel), joern.peckmann@uni-hamburg.de (J. Peckmann).

¹ Deceased.

1. Introduction

The seepage of hydrocarbon-rich, low-temperature fluids is a common phenomenon along oceanic margins in shallow as well as in deep marine environments (Suess, 2020). The hydrocarbons are composed either of short-chain hydrocarbons like methane, ethane, and propane, or higher hydrocarbons, and are accompanied by hydrogen sulfide locally produced in the seep environment (Sibuet and Olu, 1998; Smrzka et al., 2019). The seep fluids rise from the sedimentary subsurface to the seabed, where a minor fraction of the hydrocarbons can leak into the water column and the atmosphere (Chen and Feng, 2023). At seeps, the formation of authigenic carbonate occurs in the sulfate-methane transition zone (SMTZ). Such carbonate is a product of a biogeochemical process: the sulfate-driven anaerobic methane oxidation (SD-AOM), performed by anaerobic methane oxidizing archaea (ANME) and sulfatereducing bacteria (eq. 1; Hinrichs et al., 1999; Thiel et al., 1999; Boetius et al., 2000; Orphan et al., 2001). This process substantially reduces the amount of methane exiting to the water column and the atmosphere, a phenomenon referred to as the 'benthic methane filter', with the derived authigenic carbonate representing a major carbon sink (Smrzka et al., 2025). Authigenic carbonate formation at methane seeps is commonly accompanied by the precipitation of other authigenic minerals, including pyrite (Peckmann et al., 2001). Such authigenic mineral phases represent an archive of the local biogeochemical processes associated with hydrocarbon seepage and the variability of the seafloor depositional environments (Boetius et al., 2000; Thiel, 2018).

$$CH_4 + SO_4^{2-} \rightarrow HCO_3^- + HS^- + H_2O$$
 (1)

Ancient seep deposits are identified by criteria including (i) geological setting; (ii) low diversity but high abundance macrofossil assemblages, including bivalves, worm tubes, and brachiopods; (iii) recurring, complex petrographic fabrics and paragenetic sequences; (iv) ¹³C-depleted authigenic carbonate minerals; and (v) ¹³C-depleted lipid biomarkers (Peckmann et al., 2004; Campbell, 2006; Hryniewicz, 2022). Typical carbonate fabrics and phases associated with seepage are clotted micrite, crypto- to microcrystalline yellow aragonite, and fibrous aragonite cement forming isopachous rims or botryoidal crystal aggregates – the latter referred to as banded and botryoidal cement. In ancient deposits, aragonite becomes increasingly recrystallized to calcite with age (e.g., Peckmann et al., 2002; Campbell, 2006; Shapiro and Ingalls, 2025). At modern seeps, the finely crystalline pink or yellow aragonite phases have been shown to precipitate much faster than the more

coarsely crystalline fibrous aragonite cement and contain higher lipid biomarker contents than the latter (Smrzka et al., 2025). Petrographic observations combined with carbon stable isotope compositions of carbonate minerals can give an initial indication as to whether oil compounds or methane were the major carbon source for carbonate formation in ancient seep deposits (e.g., Peckmann et al., 1999; Buggisch and Krumm, 2005; Himmler et al., 2015), but should be complemented by the analysis of element patterns (Smrzka et al., 2016) and lipid biomarkers (Krake et al., 2022) for validation. Lipid biomarkers are the tool of choice for the recognition of SD-AOM in deep-time and can be preserved in thermally immature seep carbonate deposits (Wang et al., 2024) to deposits of intermediate maturity (Birgel et al., 2008b). The application of lipid biomarkers and their compound-specific δ^{13} C values has been widely implemented in the study of ancient and modern seep deposits to discriminate between various ANME communities involved in SD-AOM (e.g., Birgel et al., 2006b; Niemann and Elvert, 2008; Chevalier et al., 2011; Blumenberg et al., 2015; Miyajima and Jenkins, 2022; Zhang et al., 2023). Kuhnpasset in northeast Greenland is one of the five sites in today's Arctic area where Cretaceous-aged hydrocarbon seepage has been discovered (cf. Beauchamp and Savard, 1992; Kelly et al., 2000; Hammer et al., 2011; Hryniewicz et al., 2015; Fig. 1A), but only one Arctic site has previously published lipid biomarker data (Williscroft et al., 2017).

Here we present an integrated lipid biomarker, petrographic, and stable isotopic study of a subset of carbonate deposits from the Barremian Kuhnpasset Beds of Wollaston Forland in northeast Greenland, which have previously been described only in terms of their stratigraphic and paleontological characteristics (Kelly et al., 2000; Bjerager et al., 2020; Bang et al., 2022). The data prove conclusively that most (but not all) of the studied Kuhnpasset carbonates were formed by the seepage of methane. Further, compared to other Mesozoic seep deposits (e.g., Peckmann et al., 1999; Birgel et al., 2006a, 2006b), the preservation of lipid biomarkers in the Kuhnpasset seep deposits is extraordinary and allows a precise assignment of the predominate SD-AOM consortium and the source of methane. One motivation of this study is therefore to unravel the factors responsible for the excellent preservation of biomarkers in the studied deposits. Moreover, the Kuhnpasset seep carbonates contain substantial quantities of wood fragments and other plant remains, allowing us to investigate a potential relationship between the Kuhnpasset chemosynthesis-based SD-AOM communities and the entrained wood fragments.

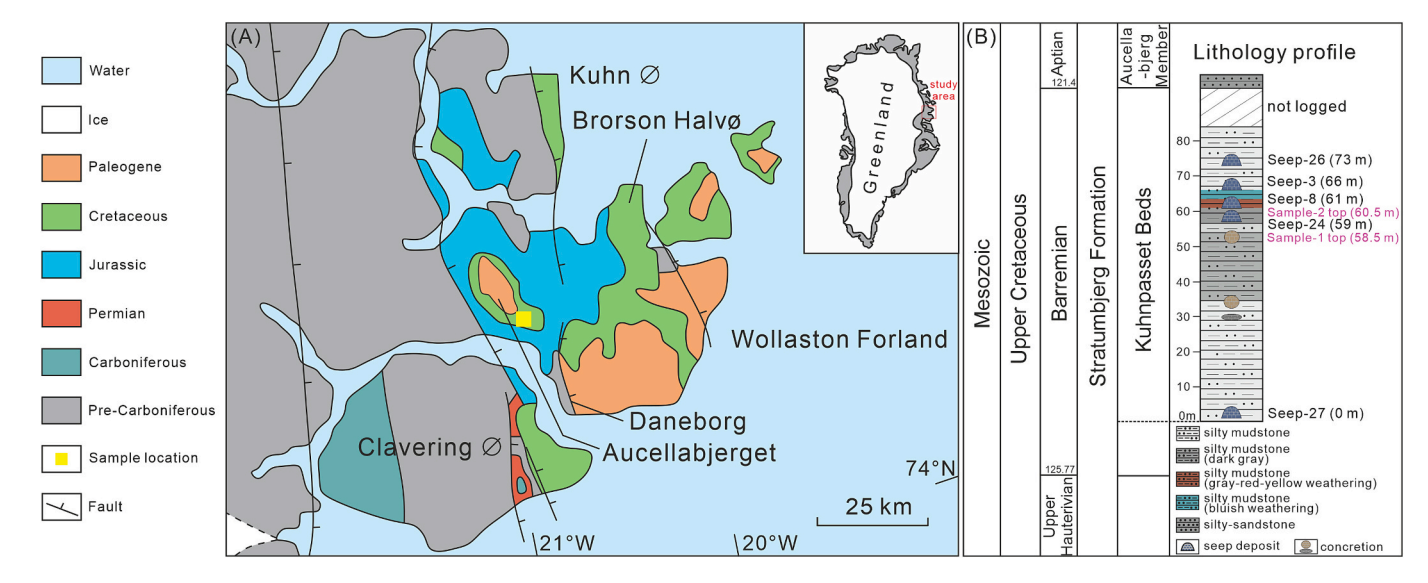


Fig. 1. (A) Schematic geological map of the study site Wollaston Forland, northeast Greenland (modified from Bjerager et al., 2020; Bang et al., 2022); (B) Stratigraphic column and lithology profile of Kuhnpasset Beds (based on Kelly et al., 2000; Bang et al., 2022 and new data).

2. Geological setting and sample collection

The geological setting of the Kuhnpasset seep deposits was first described by Kelly et al. (2000), who named the enclosing sedimentary strata the Kuhnpasset Beds. This unit was later incorporated into the Barremian-Albian aged Stratumbjerg Formation (Bjerager et al., 2020). Bang et al. (2022) investigated the palynology of the seep carbonates and the enclosing silty and sandy mudstones, and based on dinoflagellate cysts, assigned them to an? early-late Barremian age range. The Kuhnpasset seep deposits number more than 30 and all but one are exposed on a ridge on the eastern side of Kuhnpasset over an area of ca. 1 km² below the western flank of Aucellabjerget Mountain (Fig. 1). They co-occur with carbonate-cemented concretions of various sizes and shapes (Kelly et al., 2000; Bang et al., 2022. Kelly et al., 2000) gave numbers to most of the individual seep deposits, which vary in size from 1 to 3 m in diameter and are up to 1.8 m in height. They have lenticular or elliptical shapes, with relatively flat bases, where exposed. The interiors of the seep deposits are characterized in hand specimen by complex carbonate cements and vugs, and contain large fossils, including the bivalves Caspiconcha whithami, Amanocina kuhnpassetensis, Solemya sp., and the wood-boring genus Turnus, gastropods, and nektonic cephalopods (Kelly et al., 2000).

The samples for this study were collected during fieldwork to Kuhnpasset between the 2nd and 12th August 2019 by CTSL, HAN, and SRAK under Prospecting License No. 2017/15 from the Ministry of Industry, Energy and Research, Government of Greenland. These samples come from Seep-27, Seep-24, Seep-8, Seep-3, and Seep-26 of Kelly et al. (2000), with Seep-27 being the lowest stratigraphically in the Kuhnpasset section (Fig. 1B). We also included in the study material from Seep-1 and Seep-2 of Kelly et al. (2000), which we call here Sample-1 and Sample-2, as the petrographic and stable isotopic data presented below indicates that these are not seep-related.

3. Methods

3.1. Petrography and stable isotope composition of carbonates

Subsets of samples Seep-27, Seep-24, Seep-8, Seep-3, Seep-26, and Sample-1 were prepared for 30 to 35 μm -thick uncovered petrographic thin sections. Seventy-five thin sections were investigated and photographed in plane-polarized and cross-polarized light using a Leica DMLB microscope and photographed with a Leica MC170HD digital camera. Illustrated thin sections (Fig. 2) are deposited in the paleontological collections of the Natural History Museum, University of Oslo (PMO).

A total of 32 powders from Seep-27, Seep-24, Seep-8, Seep-3, Seep-26, Sample-1, and Sample-2 were analyzed for their stable isotope compositions ($\delta^{13}C$ and $\delta^{18}O$) at the Department of Earth Science, University of Bergen, Norway. The powders were obtained by drilling on cut surfaces with a 1 mm drill bit. They were analyzed using Finnigan MAT251 and MAT253 machines coupled to automated Kiel devices; the data are reported to V-PDB standard; the long-term analytical precision is 0.05 % with respect to $\delta^{13}C$ and 0.1 % with respect to $\delta^{18}O$ values.

3.2. Lipid biomarker analysis

Samples from Seep-27, Seep-24, Seep-8, Seep-3, Sample-2, and Sample-1 used for lipid biomarker analyses had an average weight of 160 g and were cleaned by bathing the rock first in 10 % hydrochloric acid and afterwards in acetone. The cleaned samples were broken up into small pieces and dissolved with 10 % hydrochloric acid. The residual material after dissolution was centrifuged and then saponified with 6 % KOH in methanol after addition of internal standards and was extracted repeatedly with a mixture of dichloromethane:methanol (3:1; v:v) until the solvents became colorless. The resulting saponification extracts were combined with the total lipid extracts (TLE). Water was added to the combined extract and the aqueous phase was acidified to

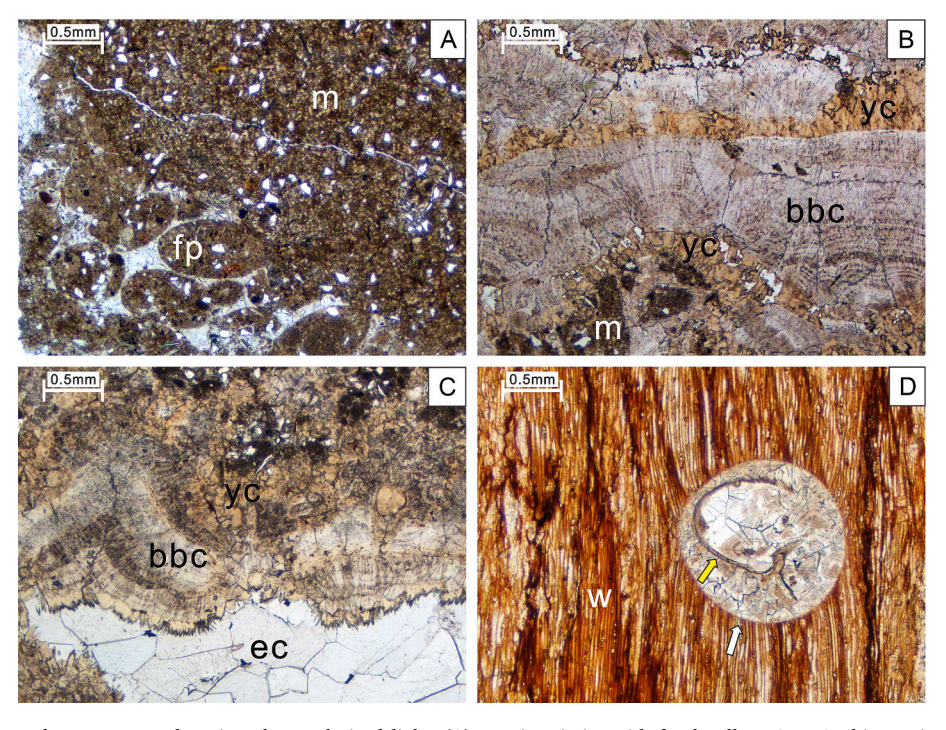


Fig. 2. Petrography of the Kuhnpasset seep deposits, plane-polarized light. (A) Matrix micrite with fecal pellets; Seep-3; thin section PMO 222.048. (B) Early diagenetic carbonate phases, multiple alternations of yellow calcite with banded and botryoidal cement; Seep-8; thin section PMO 222.099A. (C) Paragenetic sequence of micrite, yellow calcite, banded and botryoidal cement, and equant calcite cement; Seep-8; thin section PMO 222.098. (D) Wood fragment with a carbonate cement-filled *Teredolites* boring (white arrow; yellow arrow points to the shell of a wood-boring bivalve, most likely *Turnus* sp.); Seep-3; thin section PMO 222.077B. m, micrite; fp, fecal pellets; yc, yellow calcite; bbc, banded and botryoidal cement; ec, equant calcite cement; w, wood fragment. (For interpretation of the references to colour in this figure legend, the reader is referred to the web version of this article.)

pH 2 to release free fatty acids. The resulting TLE including fatty acids was separated with the aid of the solvents *n*-hexane and dichloromethane into maltenes and asphaltenes, respectively. The maltene fraction was separated by column chromatography (SPE Chromabond, NH₂, 500 mg) into hydrocarbons, ketones, alcohols, and fatty acids. The alcohol and fatty acid fractions were derivatized with N,O-bis (trimethylsilyl) trifluoroacetamide:pyridine (1:1; v:v) and 10 % boron trifluoride in methanol (1:8; v:v), respectively. The detailed decarbonization and extraction procedures have been described in Birgel et al. (2006b, 2008a). The alcohol fractions did not contain any pristine compounds and are not further discussed below. Sample-1 and Sample-2 did not contain lipid biomarkers of the SD-AOM consortium (Supplementary Fig. S1, S2), so were not further analyzed.

Aliquots of the asphaltene fraction were desulfurized using 8 ml tetrahydrofuran:methanol (1:1; v:v) mixed with 200 mg water-free nickel (II)-chlorid (NiCl₂) and 200 mg sodium boronhydride (NaBH₄), then repeatedly extracted with dichloromethane:methanol (1:1; v:v) collecting the resulting products with MilliQ water and dichloromethane. The resulting hydrocarbon fractions were separated from the polar fractions using a silica gel column. The detailed desulfurization procedure followed Schouten et al. (1993) and Sabino et al. (2021).

All fractions were analyzed with gas chromatography–mass spectrometry (GC–MS) using a Thermo Scientific Trace GC Ultra gas chromatograph coupled to a Thermo Scientific DSQ II mass spectrometer at University of Hamburg. Quantification of lipid biomarkers was achieved with a Thermo Scientific Trace GC 1310 gas chromatography (GC) coupled with a flame ionization detection (FID). The GC–MS devices were equipped with 30 m TG-5MS fused silica capillary column (0.25 mm i.d., 0.25 μm film thickness) and helium was used as carrier gas. The GC temperature program was set to 50 °C (for 3 min) ramping up to 325 °C at 6 °C/min, and 25 min isothermal. The identification of compounds was based on comparison of mass spectra and GC retention times with published data.

The two co-eluting isoprenoids crocetane and phytane cannot be separated by gas chromatography with the applied conditions on the GC. An estimate of the relative proportions of the co-eluting isoprenoids was provided by extracting the masses m/z 169 (crocetane) and m/z 183 (phytane) from the total ion current. Subsequently, the peak areas of the two masses were summed up, and relative percentages of the respective peak areas were calculated (Table 1).

For compound-specific carbon isotope measurement, a gas chromatograph (Agilent 6890) coupled with a Thermo Finnigan Combustion III interface to a Thermo Finnigan MAT 253 isotope mass spectrometer (GC-IRMS) was used at University of Bremen. The GC conditions were as follows: 50 °C (for 2 min) to 320 °C at 12 °C/min. Carbon stable isotope composition is expressed as δ^{13} C values relative to the V-PDB standard. The standard deviation of replicate measurements was within ± 0.8 ‰.

4. Results

4.1. Petrography

Samples from Seep-27, Seep-24, Seep-8, and Seep-3 exhibit a similar paragenetic sequence of carbonate phases, typified by the abundance of early diagenetic carbonate cements. The dominant carbonate phases are (i) matrix micrite, (ii) yellow calcite, (iii) fibrous cement forming banded and botryoidal crystal aggregates, and (iv) equant calcite cement. The matrix of the deposits is dominated by a dark, brownish micrite with abundant detrital grains, especially quartz and feldspars. Parts of the deposits, including the micritic matrix, have been recrystallized to different degrees to microspar. Peloids, interpreted to represent fecal pellets, are abundant in Seep-27, Seep-24, Seep-8, and Seep-3 and are mainly found in the micritic matrix (Fig. 2A). Yellow calcite postdates micrite and is typically closely associated with the banded and botryoidal cement. It commonly occurs as irregular interlayers of banded and botryoidal cement (Fig. 2B). Banded and botryoidal cement

is commonly the volumetrically dominant carbonate phase and forms regularly cement rims (Fig. 2B, C). The latest stage phase comprises equant calcite cement, which fills up the remaining cavity and pore space, and replaces in some areas the earlier cement phases (Fig. 2C). Wood fragments are common; they are up to 9 mm in diameter and are enclosed in micritic matrix and commonly filled by authigenic carbonate (Fig. 2D). Some wood fragments have *Teredolites* trace fossils, made by wood-boring bivalves (Kelly, 1988; Kelly et al., 2000). Sample-2 comprised micrite and some patches of equant calcite cement; Sample-1 had micrite only.

4.2. Carbon and oxygen stable isotopes

The analyzed carbonates have $\delta^{13} \text{C}$ values between -54.2 and -4.9% and $\delta^{18} \text{O}$ values between -12.7 and +3.2% (Fig. 3, Supplementary Table S1). Micrite is typified by $^{13} \text{C}$ -depletion with values varying from -51.3 to -6.8%; peloidal micrite yielded low $\delta^{13} \text{C}$ values of around -51%. Banded and botryoidal cement shows the most negative $\delta^{13} \text{C}$ values of all carbonate phases, varying from -54.2 to -29.7%. $\delta^{18} \text{O}$ values of micrite and banded and botryoidal cement range from -11.3 to +3.2%; only sample Seep-24 yielded positive $\delta^{18} \text{O}$ values. Equant calcite cement yielded the least negative $\delta^{13} \text{C}$ values, ranging from -36.9 to -9.9% and relatively uniform $\delta^{18} \text{O}$ values with an average of around -11%. The Caspiconcha shell samples has $\delta^{13} \text{C}$ values of -5.7 and -4.9% and $\delta^{18} \text{O}$ values of -0.1 and 1.0%.

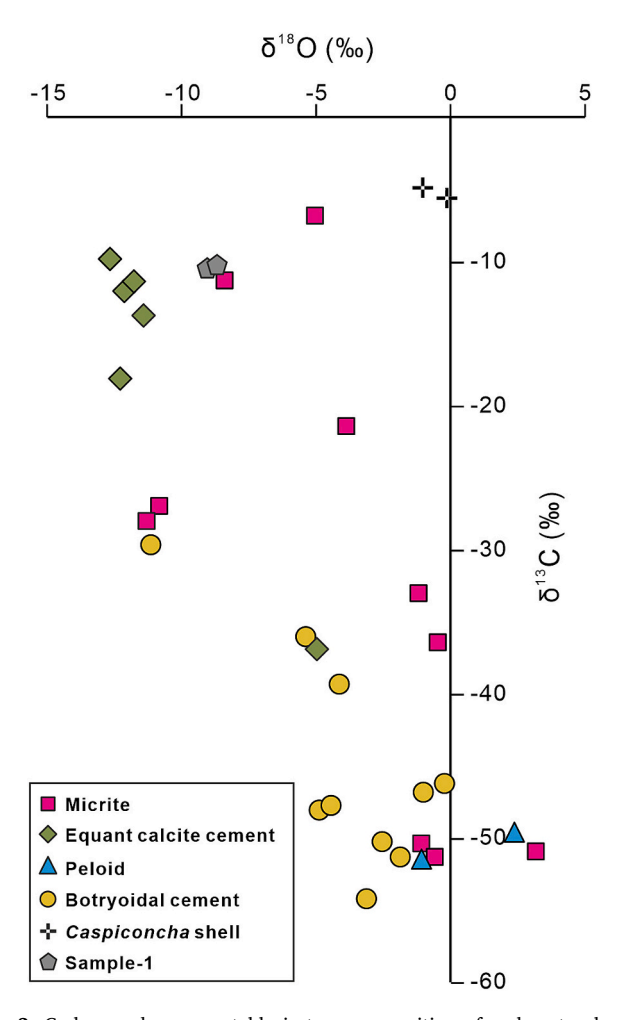


Fig. 3. Carbon and oxygen stable isotope composition of carbonate phases. Values are relative to V-PDB standard.

4.3. Lipid biomarker inventory

The samples from Seep-27, Seep-24, Seep-8, and Seep-3 contain significant amounts of molecules in the hydrocarbon and carboxylic acid fractions, as well as some polycyclic aromatic hydrocarbons in the aromatic fraction. All samples reveal a predominance of isoprenoids in the hydrocarbon fractions. The carboxylic acid fractions are dominated by short-chain fatty acids, mostly n-fatty acids and terminally branched fatty acids and accompanied by isoprenoic acids. Small amounts of organic sulfur compounds (OSCs) are also found in the hydrocarbon fractions of samples Seep-24, Seep-8, and Seep-3. The total contents of compounds in the hydrocarbon and carboxylic acid fractions does not vary significantly in the various samples. The total inventory of compounds and their carbon isotopic compositions are shown in Table 1.

4.3.1. Hydrocarbon fractions

The hydrocarbon fractions include minor n-alkanes, which comprise about 20 % of the total content in the hydrocarbons of samples Seep-27, Seep-24, Seep-8, and Seep-3. Generally, n-alkanes range from n- C_{14} to n- C_{29} , with short-chain n-alkanes with less than 24 carbons predominating. Among the short-chain alkanes, n- C_{16} to n- C_{19} and n- C_{23} are most abundant in all samples. The n-alkanes are accompanied by terminally branched alkanes, iso- and inteiso-alkanes ranging from i14 to i19.

The most abundant compounds in all samples are isoprenoids with an average proportion of 65 % of all hydrocarbon compounds, with the combined tail-to-tail linked C_{20} isoprenoid crocetane (2,6,11,15-

tetramethylhexadecane) and the head-to-tail linked phytane (2,6,10,14tetramethylhexadecane) peak amounting to 2639 ng/g rock (Seep-3) to 5489 ng/g rock (Seep-8); for the combined crocetane/phytane peak, crocetane accounts for 59 % and 63 %, respectively. Tail-to-tail linked 2,6,10,15,19-pentamethylicosane (PMI) reveals contents as high as 2609 ng/g rock (Seep-8), accounting for 20 % of all hydrocarbon compounds in the four samples on average. The tail-to-tail linked C₃₀ isoprenoid squalane is present in all samples with low contents of 98 to 185 ng/g rock, representing an average proportion of 1 %. Other groups of isoprenoids comprise head-to-tail linked farnesane, nor-pristane, and pristane with a total content averaging 8 % in all samples. The only head-to-tail linked pseudohomologue isoprenoid found is 2,6,10,14-tetramethylheptadecane (C21-isoprenoid) in samples Seep-24 and Seep-3, amounting to 3 % of all hydrocarbons on average. Organic sulfur compounds (OSCs) are found in the three younger samples and mainly included PMI-thianes with total contents of 164, 185, and 120 ng/g rock for the samples Seep-24, Seep-8, and Seep-3, respectively (Fig. 4).

Compound-specific δ^{13} C values of the hydrocarbon fraction vary between -124 % (pristane and mixed crocetane/phytane, sample Seep-8) and -30 % (n-C $_{20}$ -alkane, sample Seep-27). The lowest δ^{13} C value of n-alkanes is -108 % (n-C $_{14}$ -alkane, samples Seep-8 and Seep-27). Sample Seep-8 also yielded the lowest δ^{13} C values of isoprenoids, ranging from -124 % (pristane and crocetane/phytane) to -104 % (squalane), whereas the highest δ^{13} C values of isoprenoids are present in sample Seep-27 (-57 %; nor-pristane). Generally, the mixed crocetane/phytane peak and PMI are the most 13 C-depleted compounds for all

 Table 1

 Contents of selected lipid biomarkers and their compound-specific carbon stable isotope compositions.

Sample Compound	Seep-27		Seep-24		Seep-8		Seep-3	
	Content (ng/g)	δ ¹³ C (‰)						
n-alkanes								
n-C ₁₄	90	-108	27	tr	40	-108	45	-95
n-C ₁₇	831	-38	224	-57	146	-104	107	-69
n-C ₂₀	492	-30	158	-57	77	-88	109	-56
n-C ₂₃	555	-95	165	-89	153	-105	177	-81
Terminally branched alkanes								
iso-C ₁₄	68	-100	15	tr	26	tr	24	-93
anteiso-C ₁₄	34	-110	6	tr	18	tr	18	tr
iso-C ₁₅	199	-71	89	-71	108	-94	92	-76
anteiso-C ₁₅	82	tr	41	tr	60	-92	48	-70
iso-C ₁₆	159	-85	80	-90	105	-102	77	-90
anteiso-C ₁₆	140	-88	58	-89	69	-106	59	-94
iso-C ₁₇	271	-54	139	-80	90	-94	76	-93
anteiso-C ₁₇	209	-49	83	-81	81	-103	45	-95
Isoprenoids								
nor-pristane	499	-57	158	-80	196	-110	122	-101
Pristane	1206	-60	516	-92	716	-124	408	-113
crocetane/phytane (%)	4849 (54)	-105	2806 (51)	-114	5489 (63)	-124	2639 (59)	-119
C ₂₁ -isoprenoid (regular)	n.d.		211	-104	n.d.		122	со
PMI, irregular	2505	-118	1965	-113	2609	-122	1409	-117
Squalene	185	tr	98	-92	113	-104	101	tr
Branched fatty acids								
iso-C ₁₅	947	-90	996	-88	789	_99	615	-90
anteiso-C ₁₅	673	-89	620	-87	550	-98	476	-91
anteiso-/iso-C ₁₅ ratio	0.7		0.6		0.7		0.8	
10me-C ₁₆	181	−75	166	-86	151	-92	151	-90
iso-C ₁₇	523	-92	523	-90	433	-107	300	-92
anteiso-C ₁₇	324	-87	287	-91	402	-106	211	-94
Isoprenoic acids								
Phytanoic acid	1446	-101	1421	-107	1253	-112	829	-111
C ₂₁ -isoprenoic acid (regular)	241	-107	162	-104	334	-113	80	-103
PMI-acid (regular)	161	-111	129	-110	155	-120	69	-107
1 mi deid (regular)	101	-111	147	-110	100	-120	0,7	-107

ng/g, ng/g rock; tr, trace amounts; n.d., not detected; n.m., not measured due to low contents; co, co-elution; δ^{13} C values are in % vs. V-PDB; PMI-acid, 3,7,11,15,19-pentamethylicosanoic acid; numbers in brackets designate percentage of crocetane in mixture.

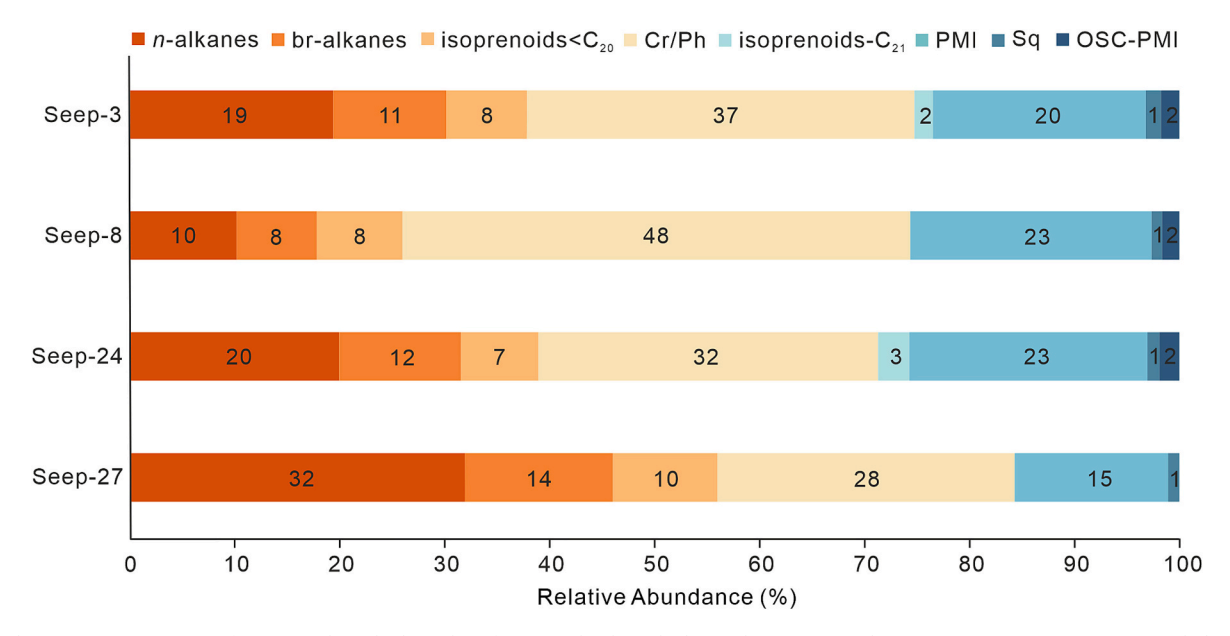


Fig. 4. Relative proportions (%) of compounds in hydrocarbon fractions. br, branched; Cr/Ph, crocetane/phytane; PMI, 2,6,10,15,19-pentamethylicosane; Sq, squalane; OSC-PMI, sulfurized PMI.

samples. The most 13 C-depleted terminally branched alkanes are *iso*- and *anteiso*-C₁₄ in sample Seep-27 with δ^{13} C values of -100 % and -110 %, respectively, followed by *iso*- and *anteiso*-C₁₆ with values of -102 % and -106 %, respectively in sample Seep-8 (Table 1, Fig. 5).

4.3.2. Carboxylic acid fractions

The n-fatty acids are the most abundant compounds in the carboxylic acid fraction with an average of 51 % of all compounds, followed by terminally branched fatty acids with an average of 30 %. The chain lengths of n-fatty acids varied from C_{12} to C_{28} , and the highest contents are found for n- C_{16} with 2495 ng/g rock in sample Seep-27. Among the branched fatty acids, iso- and anteiso- C_{15} fatty acids are the most

abundant compounds with total contents of 1417 ng/g rock on average, followed by *iso*- and *anteiso*- C_{17} with lower total average contents of 751 ng/g rock. Isoprenoic acids are found with an average content of 1671 ng/g rock; among the isoprenoids, phytanoic acid is most abundant with an average content of 1237 ng/g rock (Fig. 6). Other isoprenoic acids make up less than 3 % of the carboxylic acids.

The isoprenoic acids yielded the lowest $\delta^{13}C$ values in the carboxylic acid fraction, ranging from -115 ‰ (Seep-8) to -106 ‰ (Seep-27) on average. The lowest $\delta^{13}C$ values were obtained for head-to-tail linked 3,7,11,15,19-pentamethylicosanoic acid (PMI-acid) with values as low as -120 ‰ in sample Seep-8. Terminally branched *iso*- C_{15} and $-C_{17}$ fatty acids yielded the lowest values of -99 ‰ and -107 ‰, respectively in

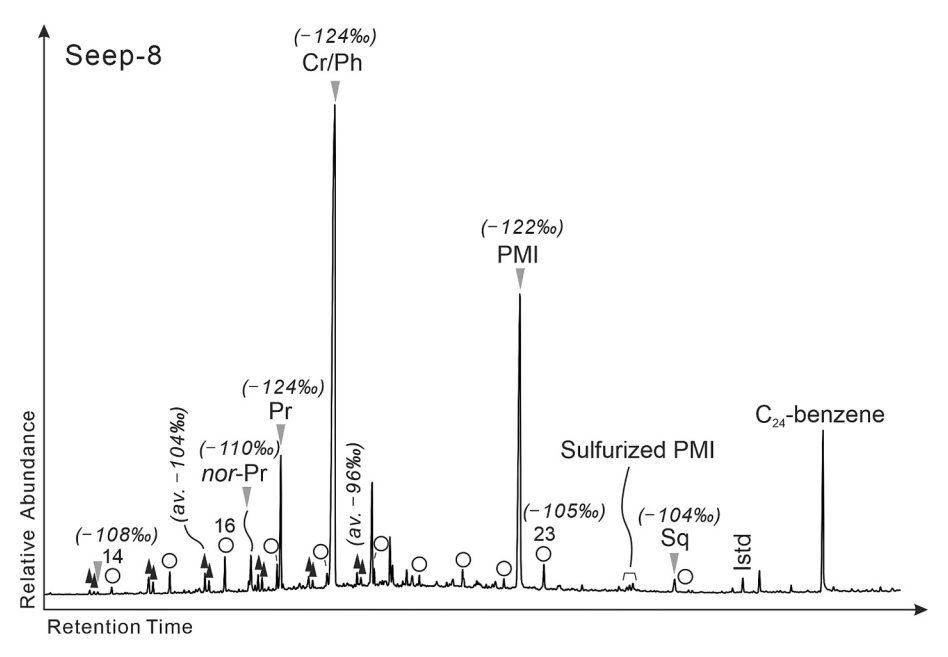


Fig. 5. Partial gas chromatogram (FID) of the hydrocarbon fraction and compound-specific carbon isotopic values (‰ vs. V-PDB) of selected compounds for sample Seep-8. White circles, *n*-alkanes with number of carbon atoms; black triangles, *iso*- and *anteiso*-alkanes; gray triangles, isoprenoids; *nor*-Pr, *nor*-pristane; Pr, pristane; Cr, crocetane; Ph, phytane; PMI, 2,6,10,15,19-pentamethylicosane; Sq, squalane; Istd, internal standard.

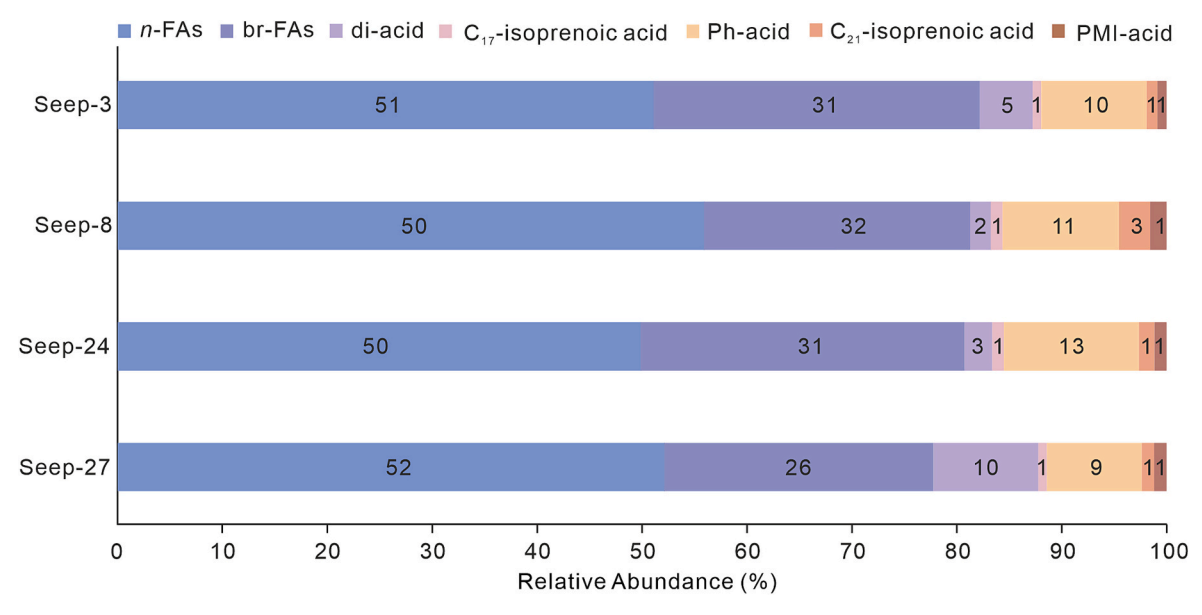


Fig. 6. Relative proportions (%) of compounds in carboxylic acid fractions. FAs, fatty acids; br, branched; Ph-acid, phytanoic acid; PMI-acid, 3,7,11,15,19-pentamethylicosanoic acid.

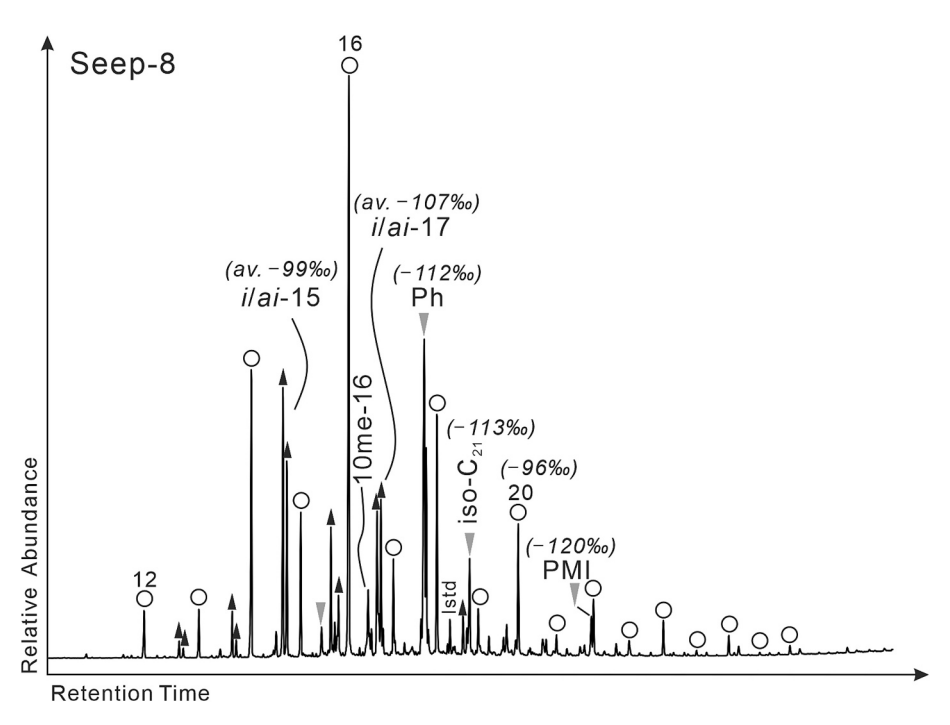


Fig. 7. Partial gas chromatogram (FID) of the carboxylic acid fraction and compound-specific carbon isotopic values (‰ vs. V-PDB) of selected compounds for sample Seep-8. White circles, *n*-fatty acids with carbon atoms; black triangles, *iso*- and *anteiso*-fatty acids; gray triangles, isoprenoic acids; 10me-16, 10me-C₁₆ fatty acid; Ph, phytanoic acid; *iso*-C₂₁, 2,6,10,14-tetramethylheptadecanoic acid; PMI, 3,7,11,15,19-pentamethylicosanoic acid; Istd, internal standard.

sample Seep-8 (Table 1, Fig. 7).

4.3.3. Aromatic compounds

Aromatic hydrocarbons are dominated by perylene and show lower amounts of pyrene, fluoranthene, phenanthrene, and other polycyclic aromatic hydrocarbons with or without methyl-groups. Perylene has contents of 157, 109, 40, and 159 ng/g rock in samples Seep-27, Seep-24, Seep-8, and Seep-3, respectively. Among the samples, perylene is the most abundant aromatic compound in samples Seep-27, Seep-24, and Seep-3, while the content of perylene in Seep-8 is quite low, and the total content of other aromatic hydrocarbon compounds is mostly below 100

ng/g rock in all samples (Fig. 8).

5. Interpretations and discussion

5.1. Carbonate microfabrics and carbon and oxygen stable isotopes

The carbonate cement facies and carbon stable isotope values of Seep-27, Seep-24, Seep-8, and Seep-3 are typical of those found in modern and ancient seep deposits, confirming the inference in Kelly et al. (2000) that the carbonate bodies containing the large bivalve fossils in the Kuhnpasset Beds were formed by hydrocarbon seepage.

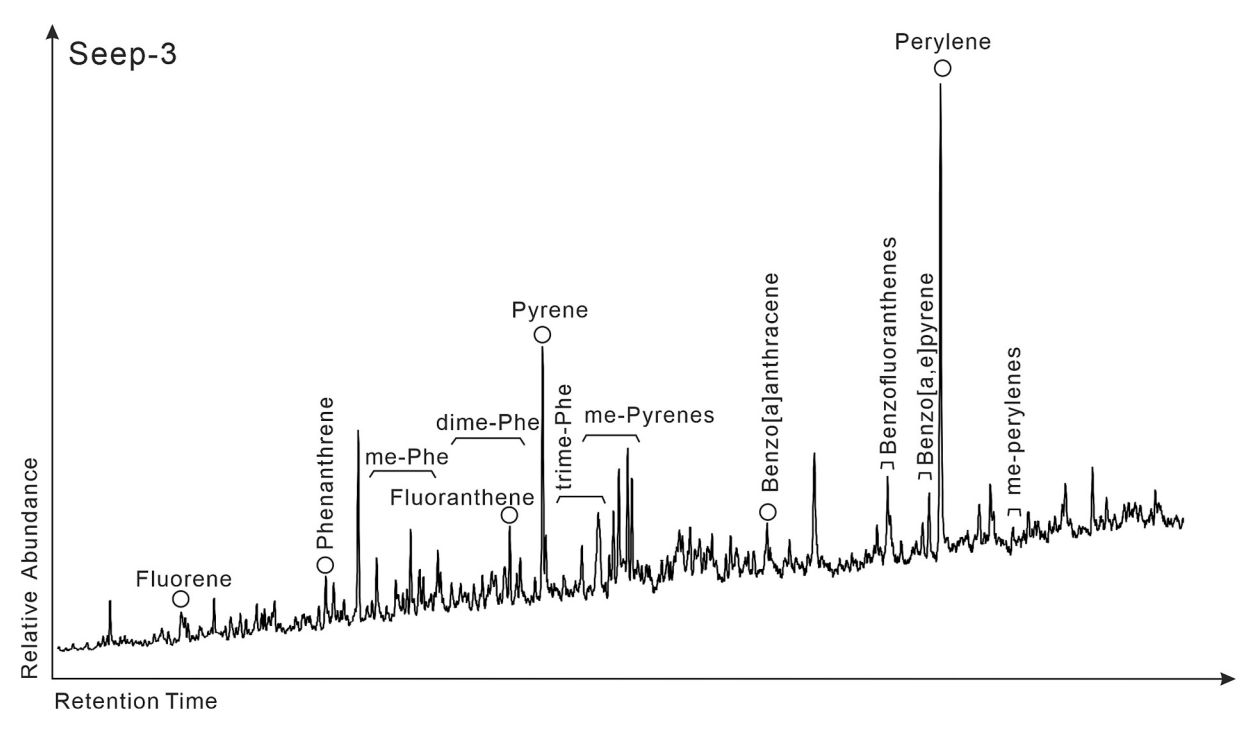


Fig. 8. Partial gas chromatogram (FID) of the aromatic fraction for sample Seep-3. Phe, phenanthrene; me-, methyl; dime-, dimethyl; trime-, trimethyl.

However, we could not confirm this for Seep-1 and Seep-2 (our Sample-1 and Sample-2) of Kelly et al. (2000), because these deposits do not have complex internal carbonate cements, and their δ^{13} C values are more typical of those of non-seep-associated carbonate concretions (cf. Raiswell and Fisher, 2000). Further, Sample-1 and Sample-2 do not contain the large bivalves found in the seep deposits, but rather a sparse bivalve fauna in common with the host sediments recorded in Kelly et al. (2000).

The evaluation of the hydrocarbon fluid composition based on δ¹³C_{carbonate} values alone is equivocal due to the fact that an unquantified mixture of different carbon sources like seawater dissolved inorganic carbon (DIC) and DIC resulting from the oxidation of sedimentary organic matter, oil-derived hydrocarbons, and methane as well as residual DIC from a pore-water pool affected by methanogenesis can produce variable isotope compositions (Himmler et al., 2008; Akam et al., 2023). Despite an unquantified degree of mixing of different carbon sources, $\delta^{13}C_{carbonate}$ values as low as -54 % of the banded and botryoidal cement from the Seep-27, Seep-24, Seep-8, and Seep-3 deposits not only confirm the presence of methane in the Kuhnpasset seepage fluids, but such low values also suggest a biogenic origin of methane (cf. Whiticar, 1999; Fig. 3). Microfabrics with less negative δ^{13} C values, as for example the matrix micrite, agree with mixed carbon sources and a higher proportion of marine DIC compared to the banded and botryoidal cements (Peckmann and Thiel, 2004; Kiel et al., 2021).

Yellow calcite, which has been interpreted to result from the recrystallization of an aragonite precursor (Zwicker et al., 2018), is abundant in many ancient seep deposits (Beauchamp and Savard, 1992; Campbell et al., 2002; Hagemann et al., 2013). Unfortunately, this phase could not be sampled separately for the analysis of $\delta^{13}C_{\text{carbonate}}$ values due to its close association with the volumetrically more abundant banded and botryoidal cement. Yellow calcite and its predecessor yellow aragonite have been interpreted as fossilized biofilms of SD-AOM consortia (Hagemann et al., 2013; Zwicker et al., 2018; Smrzka et al., 2025). In the Kuhnpasset seep deposits, yellow calcite is always closely associated with banded and botryoidal cement, commonly producing alternating sequences of the two cements. Such alternations have also been reported for modern seep deposits (Smrzka et al., 2025). The abundance of yellow calcite in all of the seep deposits studied herein is consistent with the obtained biomarker inventories, suggesting a

dominance of the ANME-2 clade, and the high contents of SD-AOM biomarkers, agreeing with the presence of abundant biofilms of SD-AOM consortia at the Kuhnpasset seeps (see chapter 5.2 for details on lipid biomarkers). The latest carbonate cement phase (equant calcite cement) exhibits less negative δ^{13} C values (-18.2 to -11.4 %) than the early cements, but still records substantial 13 C-depletion, unlike marine carbonates forming from seawater DIC. Such 13 C-depletion suggests contributions from carbon sources other than seawater DIC. Similar δ^{13} C values from equant calcite cement in other seep carbonates have been interpreted to reflect decarboxylation of organic compounds during late diagenesis (Peckmann et al., 2013).

Oxygen isotopic compositions are more easily compromised than carbon isotopic compositions during later stages of diagenesis due to the influence of burial temperature and fluid composition (Tong et al., 2016). The δ^{13} C and δ^{18} O values from the Kuhnpasset seep deposits show a common trend where the early phase micrite, and banded and botryoidal cement are less ¹⁸O-depleted and more ¹³C-depleted than later phases, which is a common pattern for ancient seep deposits (Campbell et al., 2002; Peckmann et al., 2002). The most likely explanation for the observed ¹⁸O-depletion of the later phases is an influence of meteoric water or moderately higher temperatures during late diagenesis (cf. Peckmann et al., 2002; Himmler et al., 2008; Campbell et al., 2010). A deep burial and strong thermal overprint can be excluded though since the lipid biomarker inventory does not agree with significant alteration due to thermal stress, especially when compared with other examples of Mesozoic seep deposits (Peckmann et al., 1999; Birgel et al., 2006a).

5.2. Methane seepage and SD-AOM recorded in Kuhnpasset Beds

The two tail-to-tail linked isoprenoid hydrocarbons crocetane and PMI are the most abundant compounds in almost all of the studied Kuhnpasset samples. Both molecules are accessory lipids in archaeal membranes (Salvador-Castell et al., 2019). The extremely 13 C-depleted isoprenoid lipids with values as low as -124 % allow an assignment to ANMEs that consumed biogenic methane (cf. Peckmann and Thiel, 2004). The finding that biogenic methane was the major carbon source confirms the interpretation of Kelly et al. (2000), who previously

suggested that biogenic methane was the most likely carbon source of the SD-AOM community, given the limited sediment thickness of the shallow buried Middle Jurassic to Lower Cretaceous strata in the study area. Whereas crocetane is especially abundant in ANME-2, PMI is common in all ANMEs (Blumenberg et al., 2004; Niemann and Elvert, 2008). The ANME-2-specific lipid crocetane co-elutes with phytane and shows similar δ^{13} C values as PMI, which agrees with an assignment of phytane to ANMEs as well. Based on the premise that crocetane (making up 57 % on average of the combined peak) and PMI, which are most likely derived from the same ANME source, have similarly low isotopic values, it is probable that phytane is an exclusive or close to exclusive degradation product of archaeol or sn2-hydroxyarchaeol in the Kuhnpasset samples, not deriving from allochthonous sources (cf. Birgel et al., 2006b; Xu et al., 2022). The least ¹³C-depleted combined crocetane/ phytane peak had a value of -105 % and an offset of 13 % with PMI for sample Seep-27, where other sources of phytane like chlorophyll derivatives or contributions of this compound from methanogenic archaea are possible. Probably, chlorophyll derivatives were among the sources of phytane in this case, because pristane and shorter *nor*-pristane also exhibited slightly higher δ^{13} C values and pseudohomologization of phytane as observed for other Mesozoic and Paleozoic seep deposits (cf. Birgel et al., 2008b; Blumenberg et al., 2012; Wang et al., 2024) was not

Other than these tail-to-tail linked and head-to-tail linked isoprenoid hydrocarbons, the Kuhnpasset samples also contain head-to-tail-linked phytanoic acid, which is probably a degradation product of ANMEderived glycerol diether membrane lipids like archaeol or sn2-hydroxvarchaeol (cf. Xu et al., 2022). However, the assignment of phytane and phytanoic acid to specific ANMEs is problematic because the original sn2-hydroxyarchaeol/archaeol ratio has been altered and cannot be calculated any longer (cf. Blumenberg et al., 2004). Still, the overall scarcity of n-alkanes and the presence of 13 C-depleted phytanoic acid are more consistent with an archaeal origin of both compounds than input from allochthonous sources. The $\delta^{13}C$ offset of 4 to 12 ‰ between phytanoic acid and the mixed crocetane/phytane peak may indicate that different archaeal sources have existed for the various phytanyl moieties. Additionally, head-to-tail linked PMI-acid is detected in all four samples with δ^{13} C values as low as -120 % (Seep-8). This compound possibly derived from the cleavage and subsequent oxidation of extended archaeol and extended hydroxyarchaeol (cf. Stadnitskaia et al., 2008). Similarly, the presence of ¹³C-depleted regular C₂₁-isoprenoic acid (-113 %; Seep-8) can be explained by cleavage of glycerol diether lipids comprising at least one C₂₅ isoprenoid chain (Grice et al., 1998; Birgel et al., 2006b, 2008b; Stadnitskaia et al., 2008). While the regular C21 isoprenoid was only found in small amounts in sample Seep-24, showing the same δ^{13} C value as C₂₁-isoprenoic acid, regular PMI was not identified in the Kuhnpasset samples, possibly masked by the coeluting and more abundant irregular PMI (cf. Birgel et al., 2006b).

Other diagnostic lipids of the Kuhnpasset seep carbonates are headto-head linked acyclic biphytanes (in traces in sample Seep-8), which are degradation products of glycerol dialkyl glycerol tetraethers (GDGTs) commonly produced by ANME-1 in seep environments (Birgel et al., 2008b; Schouten et al., 2013; Liu et al., 2016); though ANME-2 can also produce GDGTs in lower abundance (Elvert et al., 2005). Biphytanoic diacids, which are putative derivatives of ANME-1 that are commonly abundant in ancient seep deposits (Birgel et al., 2008a), are lacking in the Kuhnpasset samples. Their absence agrees with the predominance of ANME-2 consortia in the Kuhnpasset seeps. Unfortunately, the low volume of sulfurized PMIs found in the Seep-24, Seep-8, and Seep-3 samples precluded the analysis of compound-specific δ^{13} C values. The formation of sulfurized PMIs agrees with sulfurization of reactive precursor molecules due to high levels of hydrogen sulfide produced by intense SD-AOM and scarcity of reactive iron during early diagenesis (e. g., Sinninghe Damsté et al., 1988, 1989a, 1989b; Werne et al., 2000; Amrani, 2014) as previously suggested for sulfurized ANME biomarkers found in Permian seep deposits of Western Australia (Wang et al., 2024).

At modern seeps, ANME-2 are closely associated with their syntrophic partners in the SD-AOM consortium, sulfate-reducing bacteria of the Desulfosarcina/Desulfococcus group (Boetius et al., 2000; Elvert et al., 2003; Niemann and Elvert, 2008). Even though the Kuhnpasset samples are of Cretaceous age, the fatty acid inventory is largely unaffected by secondary input, representing a close to primary composition of the bacterial partners in SD-AOM apart from the absence of unsaturated fatty acids. The pronounced ¹³C-depleteion of the terminally branched iso- and anteiso- C_{15} and- C_{17} fatty acids with $\delta^{13}C$ values spanning from -99 to -87 % and -107 to -87 % records the utilization of methanederived carbon with only minor influence of allochthonous input. An average ratio of anteiso- over iso-C15 of 0.7 is consistent with the dominance of ANME-2-associated Desulfosarcina in the Kuhnpasset seep environment (cf. Niemann and Elvert, 2008; Birgel et al., 2011; Guan et al., 2013; Feng et al., 2014; Himmler et al., 2015). Similar to modern seep environments, sulfate-reducing bacteria other than Desulfosarcina were present in the Kuhnpasset seep environment as indicated by the occurrence of ¹³C-depleted 10me-C₁₆ fatty acid (-92 to -75 %), a compound typically associated with Desulfovibrio (Hinrichs et al., 2000; Niemann and Elvert, 2008; Chevalier et al., 2013); such strong ¹³Cdepletion of bacterial lipids is also common at modern seeps (Hinrichs et al., 2000; Elvert et al., 2003; Blumenberg et al., 2004; Himmler et al., 2015). Because of thermal alteration, the original fatty acid patterns of SD-AOM are typically more severely compromised in Mesozoic or Paleozoic seep deposits compared to what is observed for the Kuhnpasset deposits, reflected by the transformation of fatty acids to alkanes with similarly low $\delta^{13}\text{C}$ values for more thermally-mature seep deposits (Birgel et al., 2006a, 2008b; Wang et al., 2024). Only few Mesozoic seep deposits of low maturity and minor thermal overprinting show a similar preservation pattern of fatty acids (e.g., Birgel et al., 2006a; Williscroft et al., 2017) as preserved in the Kuhnpasset seep carbonates, which makes this set of samples valuable in reconstructing the predominating SD-AOM community. Interestingly, in samples Seep-27, Seep-24, and Seep-3, iso- and anteiso-C₁₅ alkanes are found but show an offset of 19, 17, and 18 % toward higher δ^{13} C values compared to the iso- and anteiso-C₁₅ fatty acids. Moreover, an offset as high as 38 % between isoand anteiso-C₁₇ alkanes and fatty acids in sample Seep-27, together with a low average ratio of anteiso-/iso-C15 alkanes of 0.5, points to some variability in the composition of the bacterial population in the Kuhnpasset seep environment (cf. Birgel et al., 2008b; Kiel et al., 2021).

The presence of 13 C-depleted n-tricosane (δ^{13} C values as low as -105 %) in the Kuhnpasset samples, a compound more abundant than other n-alkanes with a similar number of carbon atoms, is in accord with SD-AOM; n-tricosane apparently derives from bacteria involved in or associated with SD-AOM (cf. Thiel et al., 2001; Peckmann et al., 2007; Chevalier et al., 2013). This compound is accompanied by other, short chain n-alkanes (n-C₁₄ to n-C₁₈); especially n-C₁₄ alkane with an average value of -104 % and n-C₁₇ alkane with a value of -104 % in sample Seep-8 are also possibly derived from the degradation of fatty acids or alkyl glycerol ether lipids (cf. Kiel et al., 2021).

The lipid inventory of the Kuhnpasset seep deposits records a microbial community performing SD-AOM consuming biogenic methane, as evidenced by the extremely ¹³C-depleted archaeal and bacterial biomarkers. The carbon isotope offset between parent methane and ANME-2 lipids is about -50 % (cf. Niemann and Elvert, 2008); consequently, δ¹³C_{methane} values calculated for the Kuhnpasset lipids vary between -70 and -60 % (cf. Himmler et al., 2015). Further, the lipid inventory points to ANME-2 and Desulfosarcina/Desulfococcus (DSS) consortia, prokaryotes adapted to high seepage intensities. Abundant crocetane, the low abundance of biphytanes, absence of biphytanoic diacids, and low ratios of anteiso-/iso-C15 fatty acids (0.7), along with the 13Cdepleted, former aragonite cement (vellow and banded and botryoidal cement) now recrystallized to calcite (cf. Haas et al., 2010), typify ANME-2 consortia common at seafloor sites with vigorous seepage (Elvert et al., 2005; Peckmann et al., 2009). Compared to ANME-1, ANME-2 typically dwell at shallower sediment depth (Elvert et al., 2005; Knittel et al., 2005; Guan et al., 2013), resulting in carbonate authigenesis close to the sediment-water interface at times of high methane flux (Peckmann et al., 2009; Haas et al., 2010).

Methane seepage began in the early Barremian in the Kuhnpasset area, recorded by Seep-27 (Kelly et al., 2000; Bang et al., 2022; Fig. 1B). In this deposit, and over the next three million years of the Barremian, the lipid inventories and the abundance of early diagenetic fibrous cement at the seeps indicate the dominance of ANME-2-consortia, suggesting a shallow positioning of the SMTZ and a high methane flux (cf. Peckmann et al., 2009; Feng et al., 2014), leading to the establishment of a rich benthic macrofauna, including taxa that were probably chemosymbiotic (Fig. 9). The presence of abundant sunken wood and well-preserved leafy conifer shoots (Supplementary Fig. 3) indicates a location of the seeps not far from the paleo-shoreline.

5.3. Entombment of sunken wood in seep carbonate

The presence of *Teredolites* trace fossils (some definitively produced by the wood-boring genus *Turnus*) in the wood pieces in the seep deposits poses the question whether the Kuhnpasset seep deposits can, in part, also be classified as examples of wood-falls (Young et al., 2022). Fossilized wood fragments are accessory components of some ancient seep deposits (e.g., Beauchamp et al., 1989; Peckmann et al., 2002; Himmler et al., 2008; Zwicker et al., 2015). Some of the wood fragments in these deposits have been found to be bioeroded by wood-boring bivalves (Hryniewicz et al., 2016). Interestingly, sunken wood represents a predominant carbon source of marine heterotrophic organisms consuming components like hemicellulose, cellulose, and lignin, which can also be utilized by chemosynthesis-based communities (Fagervold et al., 2012).

Fossilized wood has commonly been reported to yield abundant aromatic compounds like perylene, a compound interpreted to represent a biomarker of wood-degrading fungi (Jiang et al., 2000; Bechtel et al., 2007; Grice et al., 2009; Marynowski et al., 2013). It has been confirmed that the reduction of fungal-derived perylenequinone pigments to perylene occurs during early diagenesis (Louda and Baker, 1984; Jiang et al., 2000; Grice et al., 2009). The preservation and diagenetic transformation of the precursors of perylene is restricted to reducing

conditions during deposition and burial, typically favored by either high sedimentation rates or fast entombment by authigenic carbonate (Orr and Grady, 1967; Aizenshtat, 1973; Wakeham et al., 1979; Jiang et al., 2000). For the Kuhnpasset seep deposits, excellent preservation of ¹³C-depleted ANME and bacterial lipids agrees with fast entombment, also enabling the preservation of perylene.

However, the lipid inventory – and particularly the pronounced ¹³C-depletion of individual biomarkers – of the Kuhnpasset seep carbonates reveals that wood was not the major carbon source of the local benthic microbial community. Likewise, other than perylene, no diagnostic fungal lipids were found, for example fungal steroids (cf. Leefmann et al., 2008). Therefore, wood degradation was not the major process that sustained the local benthic communities. Probably, most wood degradation had already taken place before the wood fragments were engulfed in the authigenic methane-derived carbonates at the Kuhnpasset seep sites.

6. Conclusions

Petrography, stable carbon isotopes, and lipid biomarkers of authigenic carbonate deposits from different stratigraphic positions of the Kuhnpasset Beds indicate methane seepage in a shallow marine environment of the Early Cretaceous in northeast Greenland, spanning three million years during the Barremian. The excellent preservation of lipid biomarkers compared with other Mesozoic or Paleozoic seep deposits suggests that the Kuhnpasset seep deposits were not affected by deep burial and thermal overprinting. Extremely ¹³C-depleted archaeal and bacterial lipids reveal that the Kuhnpasset seep ecosystem was based on sulfate-driven anerobic oxidation of methane (SD-AOM). The encountered lipid inventories together with the presence of abundant early diagenetic fibrous cement indicate the predominance of ANME-2 consortia adapted to high methane flux, using biogenic methane as carbon source. SD-AOM driven carbonate authigenesis resulted in the engulfment of wood fragments, suggesting, in combination with wellpreserved leafy conifer shoots, a paleogeographic position close to the ancient shoreline. The fossilized wood fragments have been biodegraded to different degrees, with most biodegradation apparently predating SD-AOM activity and carbonate authigenesis.

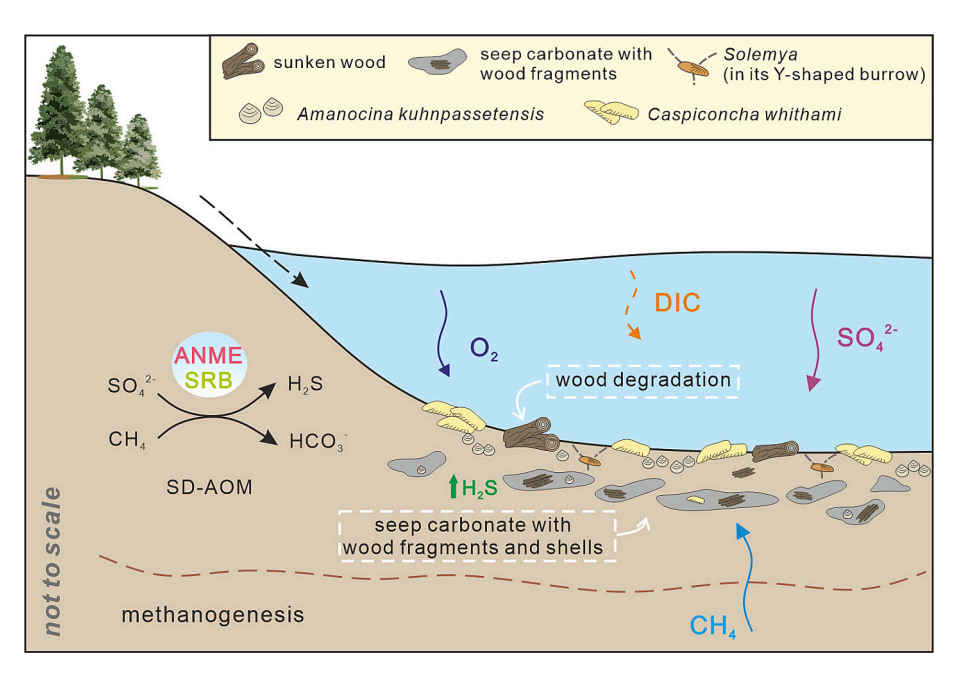


Fig. 9. Schematic diagram illustrating SD-AOM and carbonate formation at the Kuhnpasset seeps. In these nearshore, shallow-water sites, seep activity was vigorous and sunken wood and other plant material was common. DIC, dissolved inorganic carbon; ANME, anaerobic methanotrophic archaea; SRB, sulfate-reducing bacteria; SD-AOM, sulfate-driven anaerobic oxidation of methane.

CRediT authorship contribution statement

Siyu Wang: Writing – original draft, Visualization, Methodology, Investigation, Formal analysis. Daniel Birgel: Writing – review & editing, Writing – original draft, Supervision, Project administration, Investigation, Conceptualization. Hans Arne Nakrem: Writing – review & editing, Investigation, Formal analysis, Data curation. Crispin T.S. Little: Writing – review & editing, Resources, Investigation. Øyvind Hammer: Writing – review & editing, Investigation, Formal analysis. Simon R.A. Kelly: Resources. Jörn Peckmann: Writing – review & editing, Resources, Project administration, Funding acquisition, Conceptualization.

Declaration of competing interest

The authors have declared no conflict of interest.

Acknowledgments

This paper is dedicated to Simon R.A. Kelly, who sadly passed away before we could finish this project. The project fieldwork was funded by the Leverhulme Trust Grant RPG-2017-338 'Macroevolution in Boreal Ocean Jurassic-Cretaceous methane seep communities' (BOMMS). Thanks to Clive Johnson (Polarsphere), CASP (formerly Cambridge Arctic Shelf Programme), Nanok, and Dr. Peter Alsen and support staff, Geological Survey of Denmark and Greenland (GEUS) for invaluable logistical help with the fieldwork. Thanks to Brian Atkinson (University of Kansas) for plant macrofossil identifications. Joely Marie Maak (MARUM, Bremen, Germany) is thanked for extracting and processing the biomarker samples. We thank Enno Schefuß and Ralph Kreutz (both MARUM, Bremen, Germany) for GC-IRMS analyses of the samples, as well as Sabine Beckmann for support in the lab. The research was partly funded by a China Scholarship Council fellowship awarded to Siyu Wang, Insightful comments by Krzysztof Hryniewicz and two anonymous reviewers helped to improve the manuscript.

Appendix A. Supplementary data

Supplementary data to this article can be found online at https://doi.org/10.1016/j.palaeo.2025.113349.

Data availability

The authors confirm that all data necessary for supporting the scientific findings of this paper have been provided.

References

- Aizenshtat, Z., 1973. Perylene and its geochemical significance. Geochim. Cosmochim. Acta 37, 559–567. https://doi.org/10.1016/0016-7037(73)90218-4.
- Akam, S.A., Swanner, E.D., Yao, H., Hong, W.-L., Peckmann, J., 2023. Methane-derived authigenic carbonates a case for a globally relevant marine carbonate factory. Earth Sci. Rev. 243, 104487. https://doi.org/10.1016/j.earscirev.2023.104487.
- Amrani, A., 2014. Organosulfur compounds: molecular and isotopic evolution from biota to oil and gas. Annu. Rev. Earth Planet. Sci. 42, 733–768. https://doi.org/10.1146/ annurev-earth-050212-124126.
- Bang, E., Nakrem, H.A., Little, C.T.S., Kürschner, W., Kelly, S.R.A., Smelror, M., 2022. Palynology of Early Cretaceous (Barremian to Aptian) hydrocarbon (methane) seep carbonates and associated mudstones, Wollaston Forland, Northeast Greenland. Acta Palaeobot. 62, 11–23. https://doi.org/10.35535/acpa-2022-0002.
- Beauchamp, B., Savard, M., 1992. Cretaceous chemosynthetic carbonate mounds in the Canadian Arctic. Palaios 7, 434–450. https://doi.org/10.2307/3514828.
- Beauchamp, B., Harrison, J.C., Nassichuk, W.W., Krouse, H.R., Eliuk, L.S., 1989.
 Cretaceous cold-seep communities and methane-derived carbonates in the Canadian Arctic. Science 244, 53–56. https://doi.org/10.1126/science.244.4900.53.
- Bechtel, A., Widera, M., Sachsenhofer, R.F., Gratzer, R., Lücke, A., Woszczyk, M., 2007. Biomarker and stable carbon isotope systematics of fossil wood from the second Lusatian lignite seam of the Lubstów deposit (Poland). Org. Geochem. 38, 1850–1864. https://doi.org/10.1016/j.orggeochem.2007.06.018.
- Birgel, D., Peckmann, J., Klautzsch, S., Thiel, V., Reitner, J., 2006a. Anaerobic and aerobic oxidation of methane at Late Cretaceous seeps in the Western Interior

- Seaway, USA. Geomicrobiol. J. 23, 565–577. https://doi.org/10.1080/
- Birgel, D., Thiel, V., Hinrichs, K.-U., Elvert, M., Campbell, K.A., Reitner, J., Farmer, J.D., Peckmann, J., 2006b. Lipid biomarker patterns of methane-seep microbialites from the Mesozoic convergent margin of California. Org. Geochem. 37, 1289–1302. https://doi.org/10.1016/j.orggeochem.2006.02.004.Birgel, D., Elvert, M., Han, X., Peckmann, J., 2008a. ¹³C-depleted biphytanic diacids as
- Birgel, D., Elvert, M., Han, X., Peckmann, J., 2008a. ¹³C-depleted biphytanic diacids as tracers of past anaerobic oxidation of methane. Org. Geochem. 39, 152–156. https:// doi.org/10.1016/j.orggeochem.2007.08.013.
- Birgel, D., Himmler, T., Freiwald, A., Peckmann, J., 2008b. A new constraint on the antiquity of anaerobic oxidation of methane: Late Pennsylvanian seep limestones from southern Namibia. Geology 36, 543–546. https://doi.org/10.1130/G24690A.1.
- Birgel, D., Feng, D., Roberts, H.H., Peckmann, J., 2011. Changing redox conditions at cold seeps as revealed by authigenic carbonates from Alaminos Canyon, northern Gulf of Mexico. Chem. Geol. 285, 82–96. https://doi.org/10.1016/j. chemgeo.2011.03.004.
- Bjerager, M., Alsen, P., Bojesen-Koefoed, J., Fyhn, M.B.W., Hovikoski, J., Ineson, J., Nøhr-Hansen, H., Nielsen, L.H., Piasecki, S., Vosgerau, H., 2020. Cretaceous lithostratigraphy of North-East Greenland. Bull. Geol. Soc. Den. 68, 37–93. https://doi.org/10.37570/bgsd-2020-68-04.
- Blumenberg, M., Seifert, R., Reitner, J., Pape, T., Michaelis, W., Hayes, J.M., 2004. Membrane lipid patterns typify distinct anaerobic methanotrophic consortia. Proc. Natl. Acad. Sci. U. S. A. 101, 11111–11116. https://doi.org/10.1073/pnas.0401188101.
- Blumenberg, M., Seifert, R., Buschmann, B., Kiel, S., Thiel, V., 2012. Biomarkers reveal diverse microbial communities in black smoker sulfides from Turtle Pits (Mid-Atlantic Ridge, Recent) and Yaman Kasy (Russia, Silurian). Geomicrobiol J. 29, 66–75. https://doi.org/10.1080/01490451.2010.523445.
- Blumenberg, M., Walliser, E.-O., Taviani, M., Seifert, R., Reitner, J., 2015. Authigenic carbonate formation and its impact on the biomarker inventory at hydrocarbon seeps

 a case study from the Holocene Black Sea and the Plio-Pleistocene Northern
 Apennines (Italy). Mar. Petrol. Geol. 66, 532–541. https://doi.org/10.1016/j.marnetgeo.2015.05.013.
- Boetius, A., Ravenschlag, K., Schubert, C.J., Rickert, D., Widdel, F., Gieseke, A., Amann, R., Jørgensen, B.B., Witte, U., Pfannkuche, O., 2000. A marine microbial consortium apparently mediating anaerobic oxidation of methane. Nature 407, 623–626. https://doi.org/10.1038/35036572.
- Buggisch, W., Krumm, S., 2005. Palaeozoic cold seep carbonates from Europe and North Africa—an integrated isotopic and geochemical approach. Facies 51, 566–583. https://doi.org/10.1007/s10347-005-0005-5.
- Campbell, K.A., 2006. Hydrocarbon seep and hydrothermal vent paleoenvironments and paleontology: past developments and future research directions. Palaeogeogr. Palaeoclimatol. Palaeoecol. 232, 362–407. https://doi.org/10.1016/j.palaeo.2005.06.018.
- Campbell, K.A., Farmer, J.D., Des Marais, D., 2002. Ancient hydrocarbon seeps from the Mesozoic convergent margin of California: carbonate geochemistry, fluids and palaeoenvironments. Geofluids 2, 63–94. https://doi.org/10.1046/j.1468-8123 2002 00022 x
- Campbell, K.A., Nelson, C.S., Alfaro, A.C., Boyd, S., Greinert, J., Nyman, S., Grosjean, E., Logan, G.A., Gregory, M.R., Cooke, S., Linke, P., Milloy, S., Wallis, I., 2010. Geological imprint of methane seepage on the seabed and biota of the convergent Hikurangi Margin, New Zealand: box core and grab carbonate results. Mar. Geol. 272, 285–306. https://doi.org/10.1016/j.margeo.2010.01.002.
- Chen, D., Feng, D. (Eds.), 2023. South China Sea Seeps. Springer Nature Singapore, Singapore. https://doi.org/10.1007/978-981-99-1494-4.
- Chevalier, N., Bouloubassi, I., Birgel, D., Crémière, A., Taphanel, M.-H., Pierre, C., 2011. Authigenic carbonates at cold seeps in the Marmara Sea (Turkey): a lipid biomarker and stable carbon and oxygen isotope investigation. Mar. Geol. 288, 112–121. https://doi.org/10.1016/j.margeo.2011.08.005.
- Chevalier, N., Bouloubassi, I., Birgel, D., Taphanel, M.-H., López-García, P., 2013. Microbial methane turnover at Marmara Sea cold seeps: a combined 16S rRNA and lipid biomarker investigation. Geobiology 11, 55–71. https://doi.org/10.1111/gbi.12014.
- Elvert, M., Boetius, A., Knittel, K., Jørgensen, B.B., 2003. Characterization of specific membrane fatty acids as chemotaxonomic markers for sulfate-reducing bacteria involved in anaerobic oxidation of methane. Geomicrobiol. J. 20, 403–419. https:// doi.org/10.1080/01490450303894.
- Elvert, M., Hopmans, E.C., Treude, T., Boetius, A., Suess, E., 2005. Spatial variations of methanotrophic consortia at cold methane seeps: Implications from a highresolution molecular and isotopic approach. Geobiology 3, 195–209. https://doi. org/10.1111/j.1472-4669.2005.00051.x.
- Fagervold, S.K., Galand, P.E., Zbinden, M., Gaill, F., Lebaron, P., Palacios, C., 2012. Sunken woods on the ocean floor provide diverse specialized habitats for microorganisms. FEMS Microbiol. Ecol. 82, 616–628. https://doi.org/10.1111/ j.1574-6941.2012.01432.x.
- Feng, D., Birgel, D., Peckmann, J., Roberts, H.H., Joye, S.B., Sassen, R., Liu, X.-L., Hinrichs, K.-U., Chen, D., 2014. Time integrated variation of sources of fluids and seepage dynamics archived in authigenic carbonates from Gulf of Mexico Gas Hydrate Seafloor Observatory. Chem. Geol. 385, 129–139. https://doi.org/10.1016/ j.chemgeo.2014.07.020.
- Grice, K., Schouten, S., Nissenbaum, A., Charrach, J., Sinninghe Damsté, J.S., 1998. Isotopically heavy carbon in the C₂₁ to C₂₅ regular isoprenoids in halite-rich deposits from the Sdom Formation, Dead Sea Basin, Israel. Org. Geochem. 28, 349–359. https://doi.org/10.1016/S0146-6380(98)00006-0.
- Grice, K., Lu, H., Atahan, P., Asif, M., Hallmann, C., Greenwood, P., Maslen, E., Tulipani, S., Williford, K., Dodson, J., 2009. New insights into the origin of perylene

- in geological samples. Geochim. Cosmochim. Acta 73, 6531–6543. https://doi.org/
- Guan, H., Sun, Y., Zhu, X., Mao, S., Feng, D., Wu, N., Chen, D., 2013. Factors controlling the types of microbial consortia in cold-seep environments: a molecular and isotopic investigation of authigenic carbonates from the South China Sea. Chem. Geol. 354, 55–64. https://doi.org/10.1016/j.chemgeo.2013.06.016.
- Haas, A., Peckmann, J., Elvert, M., Sahling, H., Bohrmann, G., 2010. Patterns of carbonate authigenesis at the Kouilou pockmarks on the Congo deep-sea fan. Mar. Geol. 268, 129–136. https://doi.org/10.1016/j.margeo.2009.10.027.
- Hagemann, A., Leefmann, T., Peckmann, J., Hoffmann, V.-E., Thiel, V., 2013. Biomarkers from individual carbonate phases of an Oligocene cold-seep deposit, Washington State, USA. Lethaia 46, 7–18. https://doi.org/10.1111/j.1502-3931.2012.00316.x.
- Hammer, Ø., Nakrem, H.A., Little, C.T.S., Hryniewicz, K., Sandy, M.R., Hurum, J.H., Druckenmiller, P., Knutsen, E.M., Høyberget, M., 2011. Hydrocarbon seeps from close to the Jurassic-Cretaceous boundary, Svalbard. Palaeogeogr. Palaeoclimatol. Palaeoecol. 306, 15–26. https://doi.org/10.1016/j.palaeo.2011.03.019.
- Himmler, T., Freiwald, A., Stollhofen, H., Peckmann, J., 2008. Late Carboniferous hydrocarbon-seep carbonates from the glaciomarine Dwyka Group, southern Namibia. Palaeogeogr. Palaeoclimatol. Palaeoecol. 257, 185–197. https://doi.org/ 10.1016/j.palaeo.2007.09.018.
- Himmler, T., Birgel, D., Bayon, G., Pape, T., Ge, L., Bohrmann, G., Peckmann, J., 2015. Formation of seep carbonates along the Makran convergent margin, northern Arabian Sea and a molecular and isotopic approach to constrain the carbon isotopic composition of parent methane. Chem. Geol. 415, 102–117. https://doi.org/10.1016/j.chemgeo.2015.09.016.
- Hinrichs, K.-U., Hayes, J.M., Sylva, S.P., Brewer, P.G., DeLong, E.F., 1999. Methane-consuming archaebacteria in marine sediments. Nature 398, 802–805. https://doi.org/10.1038/19751
- Hinrichs, K.-U., Summons, R.E., Orphan, V., Sylva, S.P., Hayes, J.M., 2000. Molecular and isotopic analysis of anaerobic methane-oxidizing communities in marine sediments. Org. Geochem. 31, 1685–1701. https://doi.org/10.1016/S0146-6380 (00)00106-6.
- Hryniewicz, K., 2022. Ancient hydrocarbon seeps of the world. In: Kaim, A., Cochran, J. K., Landman, N.H. (Eds.), Ancient Hydrocarbon Seeps, Topics in Geobiology. Springer International Publishing, Cham, pp. 571–647. https://doi.org/10.1007/978-3-031-05623-9 20.
- Hryniewicz, K., Hagström, J., Hammer, Ø., Kaim, A., Little, C.T.S., Nakrem, H.A., 2015. Late Jurassic–Early Cretaceous hydrocarbon seep boulders from Novaya Zemlya and their faunas. Palaeogeogr. Palaeoclimatol. Palaeoecol. 436, 231–244. https://doi.org/10.1016/j.palaeo.2015.06.036.
- Hryniewicz, K., Bitner, M.A., Durska, E., Hagström, J., Hjálmarsdóttir, H.R., Jenkins, R. G., Little, C.T.S., Miyajima, Y., Nakrem, H.A., Kaim, A., 2016. Paleocene methane seep and wood-fall marine environments from Spitsbergen, Svalbard. Palaeogeogr. Palaeoclimatol. Palaeoecol. 462, 41–56. https://doi.org/10.1016/j.palaeo.2016.08.037.
- Jiang, C., Alexander, R., Kagi, R.I., Murray, A.P., 2000. Origin of perylene in ancient sediments and its geological significance. Org. Geochem. 31, 1545–1559. https:// doi.org/10.1016/S0146-6380(00)00074-7.
- Kelly, S.R., 1988. Cretaceous wood-boring bivalves from western Antarctica with a review of the Mesozoic Pholadidae. Palaeontology 31, 341–372.
- Kelly, S.R.A., Blanc, E., Price, S.P., Whitham, A.G., 2000. Early Cretaceous giant bivalves from seep-related limestone mounds, Wollaston Forland, Northeast Greenland. Geol. Soc. Lond. Spec. Publ. 177, 227–246. https://doi.org/10.1144/GSL. SP.2000.177.01.13.
- Kiel, S., Birgel, D., Lu, Y., Wienholz, D., Peckmann, J., 2021. A thyasirid-dominated methane-seep deposit from Montanita, southwestern Ecuador, from the Oligocene-Miocene boundary. Palaeogeogr. Palaeoclimatol. Palaeoecol. 575, 110477. https:// doi.org/10.1016/j.palaeo.2021.110477.
- Knittel, K., Lösekann, T., Boetius, A., Kort, R., Amann, R., 2005. Diversity and distribution of methanotrophic archaea at cold seeps. Appl. Environ. Microbiol. 71, 467–479. https://doi.org/10.1128/AEM.71.1.467-479.2005.
- Krake, N., Birgel, D., Smrzka, D., Zwicker, J., Huang, H., Feng, D., Bohrmann, G., Peckmann, J., 2022. Molecular and isotopic signatures of oil-driven bacterial sulfate reduction at seeps in the southern Gulf of Mexico. Chem. Geol. 595, 120797. https://doi.org/10.1016/j.chemgeo.2022.120797.
- Leefmann, T., Bauermeister, J., Kronz, A., Liebetrau, V., Reitner, J., Thiel, V., 2008. Miniaturized biosignature analysis reveals implications for the formation of cold seep carbonates at Hydrate Ridge (off Oregon, USA). Biogeosciences 5, 731–738. https://doi.org/10.1111/gbi.12616.
- Liu, X.L., Birgel, D., Elling, F.J., Sutton, P.A., Lipp, J.S., Zhu, R., Zhang, C., Könneke, M., Peckmann, J., Rowland, S.J., Summons, R.E., Hinrichs, K.-U., 2016. From ether to acid: a plausible degradation pathway of glycerol dialkyl glycerol tetraethers. Geochim. Cosmochim. Acta 183, 138–152. https://doi.org/10.1016/j.gca.2016.04.016.
- Louda, J.W., Baker, E.W., 1984. Perylene occurrence, alkylation and possible sources in deep-ocean sediments. Geochim. Cosmochim. Acta 48, 1043–1058. https://doi.org/ 10.1016/0016-7037(84)90195-9.
- Marynowski, L., Smolarek, J., Bechtel, A., Philippe, M., Kurkiewicz, S., Simoneit, B.R.T., 2013. Perylene as an indicator of conifer fossil wood degradation by wood-degrading fungi. Org. Geochem. 59, 143–151. https://doi.org/10.1016/j. orggeochem.2013.04.006.
- Miyajima, Y., Jenkins, R.G., 2022. Biomarkers in ancient hydrocarbon seep carbonates. In: Kaim, A., Cochran, J.K., Landman, N.H. (Eds.), Ancient Hydrocarbon Seeps, Topics in Geobiology. Springer International Publishing, Cham, pp. 47–77. https://doi.org/10.1007/978-3-031-05623-9_2.

- Niemann, H., Elvert, M., 2008. Diagnostic lipid biomarker and stable carbon isotope signatures of microbial communities mediating the anaerobic oxidation of methane with sulphate. Org. Geochem. 39, 1668–1677. https://doi.org/10.1016/j. orgeochem.2007.11.003
- Orphan, V.J., Hinrichs, K.-U., Ussler, W., Paull, C.K., Taylor, L.T., Sylva, S.P., Hayes, J. M., Delong, E.F., 2001. Comparative analysis of methane-oxidizing archaea and sulfate-reducing bacteria in anoxic marine sediments. Appl. Environ. Microbiol. 67, 1922–1934. https://doi.org/10.1128/AEM.67.4.1922-1934.2001.
- Orr, W.L., Grady, J.R., 1967. Perylene in basin sediments off southern California. Geochim. Cosmochim. Acta 31, 1201–1209. https://doi.org/10.1016/S0016-7037 (67)80058-9
- Peckmann, J., Thiel, V., 2004. Carbon cycling at ancient methane-seeps. Chem. Geol. 205, 443–467. https://doi.org/10.1016/j.chemgeo.2003.12.025.
- Peckmann, J., Thiel, V., Michaelis, W., Clari, P., Gaillard, C., Martire, L., Reitner, J., 1999. Cold seep deposits of Beauvoisin (Oxfordian; southeastern France) and Marmorito (Miocene; northern Italy): microbially induced authigenic carbonates. Int. J. Earth Sci. 88, 60–75. https://doi.org/10.1007/s005310050246.
- Peckmann, J., Reimer, A., Luth, U., Luth, C., Hansen, B.T., Heinicke, C., Hoefs, J., Reitner, J., 2001. Methane-derived carbonates and authigenic pyrite from the northwestern Black Sea. Mar. Geol. 177, 129–150. https://doi.org/10.1016/S0025-3227(01)00128-1.
- Peckmann, J., Goedert, J.L., Thiel, V., Michaelis, W., Reitner, J., 2002. A comprehensive approach to the study of methane-seep deposits from the Lincoln Creek Formation, western Washington State, USA. Sedimentology 49, 855–873. https://doi.org/ 10.1046/i.1365-3091.2002.00474.x.
- Peckmann, J., Thiel, V., Reitner, J., Taviani, M., Aharon, P., Michaelis, W., 2004.
 A microbial mat of a large sulfur bacterium preserved in a Miocene methane-seep limestone. Geomicrobiol. J. 21, 247–255. https://doi.org/10.1080/ 01490450490438757
- Peckmann, J., Senowbari-Daryan, B., Birgel, D., Goedert, J.L., 2007. The crustacean ichnofossil *Palaxius* associated with callianassid body fossils in an Eocene methaneseep limestone, Humptulips Formation, Olympic Peninsula, Washington. Lethaia 40, 273–280. https://doi.org/10.1111/j.1502-3931.2007.00026.x.
- Peckmann, J., Birgel, D., Kiel, S., 2009. Molecular fossils reveal fluid composition and flow intensity at a Cretaceous seep. Geology 37, 847–850. https://doi.org/10.1130/
- Peckmann, J., Sandy, M.R., Taylor, D.G., Gier, S., Bach, W., 2013. An Early Jurassic brachiopod-dominated seep deposit enclosed by serpentinite, eastern Oregon, USA. Palaeogeogr. Palaeoclimatol. Palaeoecol. 390, 4–16. https://doi.org/10.1016/j. palaeo.2013.01.003.
- Raiswell, R., Fisher, Q.J., 2000. Mudrock-hosted carbonate concretions: a review of growth mechanisms and their influence on chemical and isotopic composition. J. Geol. Soc. London 157, 239–251. https://doi.org/10.1144/jgs.157.1.239.
- Sabino, M., Dela Pierre, F., Natalicchio, M., Birgel, D., Gier, S., Peckmann, J., 2021. The response of water column and sedimentary environments to the advent of the Messinian salinity crisis: insights from an onshore deep-water section (Govone, NW Italy). Geol. Mag. 158, 825–841. https://doi.org/10.1017/S0016756820000874.
- Salvador-Castell, M., Tourte, M., Oger, P.M., 2019. In search for the membrane regulators of archaea. Int. J. Mol. Sci. 20, 4434. https://doi.org/10.3390/ iims20184434.
- Schouten, S., Pavlović, D., Sinninghe Damsté, J.S., De Leeuw, J.W., 1993. Nickel boride: an improved desulphurizing agent for sulphur-rich geomacromolecules in polar and asphaltene fractions. Org. Geochem. 20, 901–909. https://doi.org/10.1016/0146-6380(93)90101-G.
- Schouten, S., Hopmans, E.C., Sinninghe Damsté, J.S., 2013. The organic geochemistry of glycerol dialkyl glycerol tetraether lipids: a review. Org. Geochem. 54, 19–61. https://doi.org/10.1016/j.orggeochem.2012.09.006.
- Shapiro, R.S., Ingalls, M., 2025. Challenges to the ancient methane seep search strategy: the Bedford Canyon Formation (Middle Jurassic, Santa Ana Mountains, California). Sedimentology 72, 688–707. https://doi.org/10.1111/sed.13252.
- Sibuet, M., Olu, K., 1998. Biogeography, biodiversity and fluid dependence of deep-sea cold-seep communities at active and passive margins. Deep-Sea Res. II Top. Stud. Oceanogr. 45, 517–567. https://doi.org/10.1016/S0967-0645(97)00074-X.
- Sinninghe Damsté, J.S., Irene, W., Rijpstra, C., De Leeuw, J.W., Schenck, P.A., 1988. Origin of organic sulphur compounds and sulphur-containing high molecular weight substances in sediments and immature crude oils. Org. Geochem. 13, 593–606. https://doi.org/10.1016/0146-6380(88)90079-4.
- Sinninghe Damsté, J.S., Rijpstra, W.I.C., De Leeuw, J.W., Schenck, P.A., 1989a. The occurrence and identification of series of organic sulphur compounds in oils and sediment extracts: II. Their presence in samples from hypersaline and non-hypersaline palaeoenvironments and possible application as source, palaeoenvironmental and maturity indicators. Geochim. Cosmochim. Acta 53, 1323–1341. https://doi.org/10.1016/0016-7037(89)90066-5.
- Sinninghe Damsté, J.S., Rijpstra, W.I.C., Kock-van Dalen, A.C., De Leeuw, J.W., Schenck, P.A., 1989b. Quenching of labile functionalised lipids by inorganic sulphur species: evidence for the formation of sedimentary organic sulphur compounds at the early stages of diagenesis. Geochim. Cosmochim. Acta 53, 1343–1355. https://doi. org/10.1016/0016-7037(89)90067-7.
- Smrzka, D., Zwicker, J., Klügel, A., Monien, P., Bach, W., Bohrmann, G., Peckmann, J., 2016. Establishing criteria to distinguish oil-seep from methane-seep carbonates. Geology 44, 667–670. https://doi.org/10.1130/G38029.1.
- Smrzka, D., Zwicker, J., Misch, D., Walkner, C., Gier, S., Monien, P., Bohrmann, G., Peckmann, J., 2019. Oil seepage and carbonate formation: a case study from the southern Gulf of Mexico. Sedimentology 66, 2318–2353. https://doi.org/10.1111/ sed.12593.

- Smrzka, D., Tseng, Y., Zwicker, J., Schröder-Ritzrau, A., Frank, N., Schmitt, A.-D., Pape, T., Birgel, D., Peckmann, J., Lin, S., Bohrmann, G., 2025. Marine carbon burial enhanced by microbial carbonate formation at hydrocarbon seeps. Communications Earth & Environment 6, 7. https://doi.org/10.1038/s43247-024-01960-0.
- Stadnitskaia, A., Bouloubassi, I., Elvert, M., Hinrichs, K.-U., Sinninghe Damsté, J.S., 2008. Extended hydroxyarchaeol, a novel lipid biomarker for anaerobic methanotrophy in cold seepage habitats. Org. Geochem. 39, 1007–1014. https://doi. org/10.1016/j.orggeochem.2008.04.019.
- Suess, E., 2020. Marine cold seeps: background and recent advances. In: Wilkes, H. (Ed.), Hydrocarbons, Oils and Lipids: Diversity, Origin, Chemistry and Fate, Handbook of Hydrocarbon and Lipid Microbiology. Springer, Cham, pp. 747–767. https://doi. org/10.1007/978-3-319-90569-3 27.
- Thiel, V., 2018. Methane carbon cycling in the past: insights from hydrocarbon and lipid biomarkers. In: Wilkes, H. (Ed.), Hydrocarbons, Oils and Lipids: Diversity, Origin, Chemistry and Fate. Springer International Publishing, Cham, pp. 1–30. https://doi. org/10.1007/978-3-319-54529-5 6-1.
- Thiel, V., Peckmann, J., Seifert, R., Wehrung, P., Reitner, J., Michaelis, W., 1999. Highly isotopically depleted isoprenoids: molecular markers for ancient methane venting. Geochim. Cosmochim. Acta 63, 3959–3966. https://doi.org/10.1016/S0016-7037 (20)00177.5
- Thiel, V., Peckmann, J., Schmale, O., Reitner, J., Michaelis, W., 2001. A new straight-chain hydrocarbon biomarker associated with anaerobic methane cycling. Org. Geochem. 32, 1019–1023. https://doi.org/10.1016/S0146-6380(01)00075-4.
- Tong, H., Wang, Q., Peckmann, J., Cao, Y., Chen, L., Zhou, W., Chen, D., 2016.
 Diagenetic alteration affecting δ¹⁸O, δ¹³C and ⁸⁷Sr₂/⁸⁶Sr signatures of carbonates: a case study on Cretaceous seep deposits from Yarlung-Zangbo Suture Zone, Tibet, China. Chem. Geol. 444, 71–82. https://doi.org/10.1016/j.chemgeo.2016.10.003.
- Wakeham, S.G., Schaffner, C., Giger, W., Boon, J.J., De Leeuw, J.W., 1979. Perylene in sediments from the Namibian Shelf. Geochim. Cosmochim. Acta 43, 1141–1144. https://doi.org/10.1016/0016-7037(79)90100-5.
- Wang, S., Birgel, D., Krake, N., Shen, C., Haig, D.W., Peckmann, J., 2024. Lessons from lipid biomarkers preserved in methane-seep carbonates from the early Permian of Western Australia. Chem. Geol. 668, 122343. https://doi.org/10.1016/j. chemgeo.2024.122343.

- Werne, J.P., Hollander, D.J., Behrens, A., Schaeffer, P., Albrecht, P., Sinninghe Damsté, J. S., 2000. Timing of early diagenetic sulfurization of organic matter: a precursor-product relationship in Holocene sediments of the anoxic Cariaco Basin, Venezuela. Geochim. Cosmochim. Acta 64, 1741–1751. https://doi.org/10.1016/S0016-7037 (99)00366-X
- Whiticar, M.J., 1999. Carbon and hydrogen isotope systematics of bacterial formation and oxidation of methane. Chem. Geol. 161, 291–314. https://doi.org/10.1016/
- Williscroft, K., Grasby, S.E., Beauchamp, B., Little, C.T.S., Dewing, K., Birgel, D., Poulton, T., Hryniewicz, K., 2017. Extensive Early Cretaceous (Albian) methane seepage on Ellef Ringnes Island, Canadian High Arctic. Geol. Soc. Am. Bull. 129, 788–805. https://doi.org/10.1130/B31601.1.
- Xu, L., Guan, H., Su, Z., Liu, L., Tao, J., 2022. Diagenetic fate of glycerol ethers revealed by two novel isoprenoid hydroxyphytanyl glycerol monoethers and non-isoprenoid alkyl glycerol ethers. Org. Geochem. 163, 104344. https://doi.org/10.1016/j. orggeochem.2021.104344.
- Young, E.L., Halanych, K.M., Amon, D.J., Altamira, I., Voight, J.R., Higgs, N.D., Smith, C. R., 2022. Depth and substrate type influence community structure and diversity of wood and whale-bone habitats on the deep NE Pacific margin. Mar. Ecol. Prog. Ser. 687, 23–42. https://doi.org/10.3354/meps14005.
- Zhang, T., He, W., Liang, Q., Zheng, F., Xiao, X., Zeng, Z., Zhou, J., Yao, W., Chen, H., Zhu, Y., Zhao, J., Zheng, Y., Zhang, C., 2023. Lipidomic diversity and proxy implications of archaea from cold seep sediments of the South China Sea. Front. Microbiol. 14, 1241958. https://doi.org/10.3389/fmicb.2023.1241958.
- Zwicker, J., Smrzka, D., Gier, S., Goedert, J.L., Peckmann, J., 2015. Mineralized conduits are part of the uppermost plumbing system of Oligocene methane-seep deposits, Washington State (USA). Mar. Pet. Geol. 66, 616–630. https://doi.org/10.1016/j. marpetgeo.2015.05.035.
- Zwicker, J., Smrzka, D., Himmler, T., Monien, P., Gier, S., Goedert, J.L., Peckmann, J., 2018. Rare earth elements as tracers for microbial activity and early diagenesis: a new perspective from carbonate cements of ancient methane-seep deposits. Chem. Geol. 501, 77–85. https://doi.org/10.1016/j.chemgeo.2018.10.010.